PRACTICAL APPLICATIONS OF VISCOUS FULL-POTENTIAL CFD CODES

David Philpott*, Kevin Hackett*
***IHS Markit (ESDU), U.K.**
Keywords: *Transonic, Excrescence, Wind-tunnel, CFD*

Abstract

Full-potential codes with coupled integral boundary-layer solutions have, with the advent of fast computer with large memories, largely given way to RANS solvers. However, although they are unable to compete in the complexity of geometries that can be modelled, they have comparable accuracy and have the advantage that they can be set up and run rapidly on a modest laptop machine and give direct output of key boundary-layer parameters. This paper describes applications of such codes to wing-design, excrescence-drag evaluation and extrapolation of wind-tunnel data.

1 Introduction

The VGK, BVGK and VFP viscous full-potential codes [1], [2], [3] were developed as aerodynamic design tools for 2D aerofoil sections and simple 3D wing/body combinations. They are particularly applicable to the design of typical transonic transport aircraft configurations. They were developed before large high-speed computing facilities with large memory were available and have been largely displaced by RANS codes that are capable of dealing with much more complex geometries and are better at dealing with local flow separation. In spite of these limitations VGK and VFP predict very accurately (Fig. 1) and can deal with small regions of separation and give accurate prediction of separation boundaries. Comprehensive boundary-layer data, including shape parameter, are included in the output, which is a very useful aid to flow diagnostics.

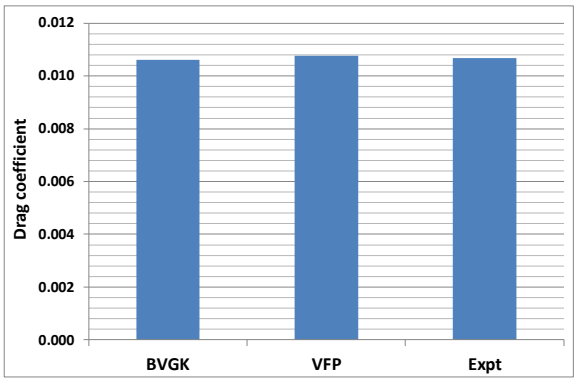

Fig. 1 Drag coefficient comparison: Centre section of a swept wing of constant chord (Section RAE 5225, $C_L = 0.403$, $M_\infty = 0.735$, $Re_c = 6.03 \times 10^6$

Compared with RANS codes these viscous full-potential codes have the advantages that they are easy to set up because gridding is automatic, their resource requirements are small, so that they can be easily accommodated on a standard laptop computer and they are fast enough to be used repetitively in optimization studies in the intermediate design phase. The integral boundary-layer representation requires specification of the transition location, which makes these codes very convenient for extrapolation of wind-tunnel results to high Reynolds numbers and, facility to impose a local increase in boundary-layer thickness on an aerofoil surface can be exploited in the evaluation of excrescence drag.

In this paper a brief description is given of the (B)VGK and VFP methods and of the three applications identified in this Section.

2 Viscous full-potential codes

The viscous full potential codes used in this work are the 2D aerofoil methods VGK [1] and

BVGK [2] (a later version with improved boundary-layer modelling) and the 3D wing/body code VFP [3].

The 2D aerofoil methods use finite difference methods to obtain a numerical solution of the full potential equations but the use of a partially conservative scheme allows close prediction of the surface pressures on a transonic aerofoil even when weak shock waves are present (Fig. 1 and the wave drag is estimated using the methods developed by Lock [4].

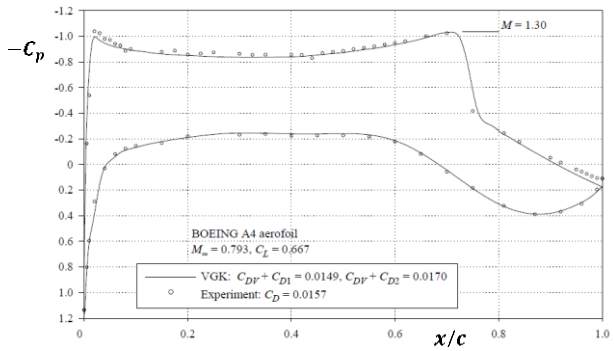

Fig. 2 Comparison of VGK with experiment (Boeing A4 section)

The integral boundary-layer (VGK and BVGK) routine uses a lag-entrainment method [5] and is solved iteratively with the potential flow equations.

Gridding is done automatically and is very rapid. The aerofoil is conformally mapped onto the computational plane, which is circular, the aerofoil surface being mapped onto its circumference and the free stream at infinity to the centre. This corresponds to an 'O' grid in the physical plane (Fig. 3).

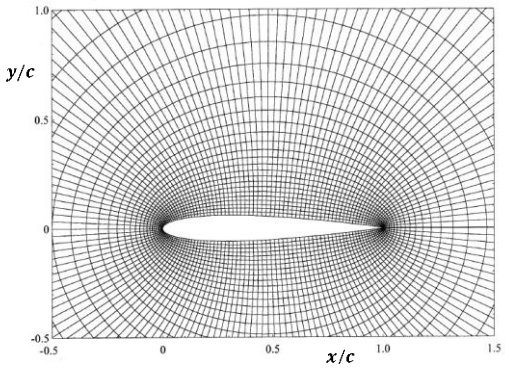

Fig. 3 VGK grid

VFP extends the methods of VGK and BVGK to 3D and the isolated wing or wing/body combinations can be modelled. The body is represented by an infinite cylinder although the effect of a finite length body can be simulated by imposing appropriate changes to the spanwise freestream Mach number distribution. The vertical position at which the wing is mounted can be varied. Gridding is similar to that used for the 2D aerofoil except that the flow field is mapped into a cylinder, rather than a circle, to allow for the third dimension. The mapping is extended beyond the wing tip, which must be approximated as a straight line. The flow solver is again similar to the 2D case except that the 3D potential-flow equations are solved. The boundary-layer method incorporates corrections for sweep and taper.

The version of VFP described in [3] and its associated documents allows easy input of data for wings with single or multiple leading and trailing edge cranks, dihedral *etc.* and has been successfully applied to forward swept wings and blended wing/body configurations.

Both the (B)VGK and VFP have been extensively evaluated against experimental data [1], [3].

3 Design applications

The design of a typical transport wing is a multi-discipline optimisation problem involving tradeoff between aerodynamic performance, structural weight *etc.* Constraints are imposed by such factors as incorporation of high-lift devices, internal storage requirements for fuel (and associated equipment such as pipes and pumps), undercarriage stowage and control actuators. There may also be additional factors, *e.g.* span limitations dictated by ground handling.

Cruise aerodynamic design is directed at ensuring good performance with acceptable off-design performance. The relative weight given to cruise performance and other factors depends on the intended mission profile of the aircraft.

Aerodynamic-prediction tools used in the initial design process should be sufficiently fast to deal with the repetitive calculations required

to cover the design space over which optimisation is to be performed and changes in aerofoil section and planform geometry should be easily accommodated. Methods used to optimise cruise performance should predict lift and drag with sufficient accuracy to allow local and global optima to be identified and should be capable of identifying drag divergence and separation boundaries to ensure acceptable off-design limits.

3.1 Aerofoil section design (VGK)

At the initial design stage of high-aspect-ratio wings, such as those on a typical transport aircraft, a suitable aerofoil section is designed and optimised to achieve the required compromise between cruise and off-design performance balancing aerodynamic and structural considerations together with other constraints. Reference [6] gives an example of the use of the VGK code in a cruise-aerodynamics optimisation study of a sonic-plateau aerofoil. The use of high-fidelity CFD is rejected as impractical because of computational demands. The use of VGK permits a large number of runs to be made (typically under 1 second per run on a standard desktop processor [6]) to establish detailed drag-divergence, separation and critical- Mach- number boundaries.

3.2 3D wing design (VFP)

The chosen aerofoil section(s) are then imported into VFP, which allows easy adjustment of planform, twist and dihedral to obtain the optimised compromise between spanwise loading and wing off-design performance constraints, *e.g.* separation boundary (Fig. 4).

As a result of these initial studies changes may be required. For example changes may be required to either local aerofoil sections or to the twist distribution to improve the separation boundary along the wing. Because of the low computational requirements of the codes, repetitive iteration of the complete aerofoil section and 3D wing-design cycles are possible.

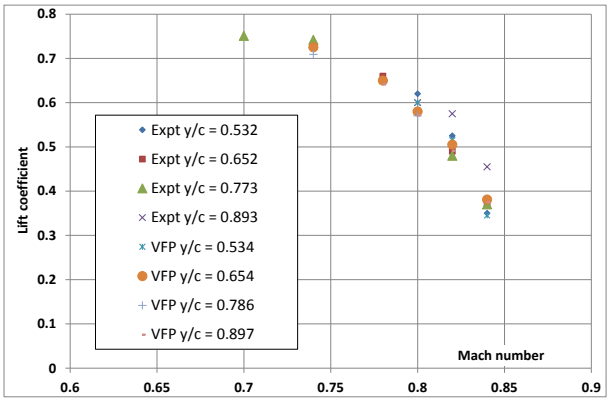

Fig. 4 VFP prediction of separation boundary compared with experiment (RAE W4 wing Re_c = 5 x 10^6, transition at 5%

Modifications may also be required near the body junction to allow for wing/body interference effects. Although VFP can only model simple bodies of circular cross section and the possible wing-mounting positions are restricted, Fig. 5, which shows the results of a calculation made using an inviscid version of the VFP code, gives an early warning of a potential problem at a wing/fuselage junction, which was confirmed by RANS calculation and experiment.

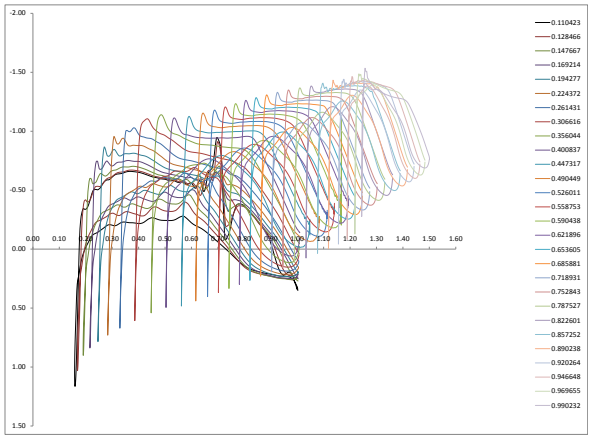

Fig. 5 Pressure distribution on F4 wing/body showing problem at wing/body junction (inviscid VFP calculation)

3.3 Unusual configurations

Although VFP was originally designed for use with conventional transonic swept wings, it has also been successfully applied to more unusual configurations such as forward-swept wings and blended wing/body (Fig. 6) configurations. It

should however, be emphasised that application to such cases should be supported by adequate validation and that adjustment may be required to default program parameters [3].

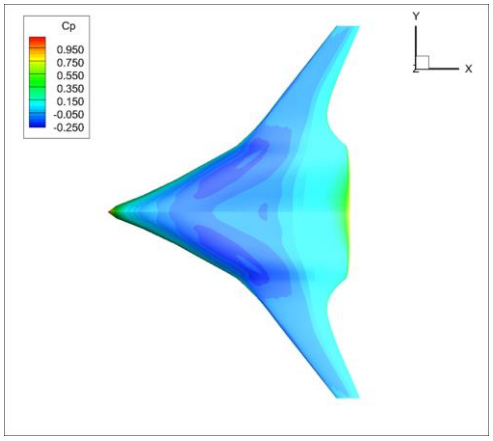

Fig. 6 Pressure coefficients on a blended wing/body (VFP calculation) (Courtesy Dr S Prince, Cranfield University)

4 Excrescence-drag calculation

The requirements for good fuel economy and low emissions are strong drivers in both the design and operation of commercial transports. Because of this drag prediction of small excrescences, such gaps and steps associated with control surfaces (Fig. 7 (a)), are of importance when specifying manufacturing and servicing tolerances. In service, repair patches may be required (Fig. 7 (b)). These must be designed in such a way that aircraft handling is not compromised and, in addition, fuel-burn penalties should be considered.

(a) **(b)**

Fig. 7 Wing excrescences: gaps associated with moveable surfaces (a) and repair patch (b)

The drag of excrescences, such as that shown in Fig. 7 (b), is estimated using basic drag data from wind-tunnel tests [7], [8] on a variety of 2D excrescences, such as grooves, ridges and forward- and backward-facing steps, from which an approximation to the actual excrescence is built up. These wind-tunnel tests were made in a uniform stream with the excrescence mounted on the tunnel sidewall.

When estimating excrescence drag on an aircraft surface, the excrescence is assumed to be located in a uniform stream with zero pressure gradient and the conditions in the uniform stream are assumed to be those at the edge of the boundary layer at the location of the excrescence but without the excrescence present. If the excrescence is located on a lifting surface, its drag may differ from the basic drag, determined from the wind tunnel tests, because of significant changes in the flow between the excrescence location and the trailing edge. These changes can be assessed using VGK [9] which allows a local increase in boundary-layer momentum thickness, directly calculated from the basic excrescence drag (measured in the wind tunnel), to be directly imposed at the excrescence location. This increase in boundary-layer thickness allows VGK to model the effect of the excrescence on the downstream flow. The ratio of the drag calculated with the imposition of the momentum thickness increment to the basic drag then gives a "magnification factor", m_d, by which the basic excrescence drag must be multiplied.

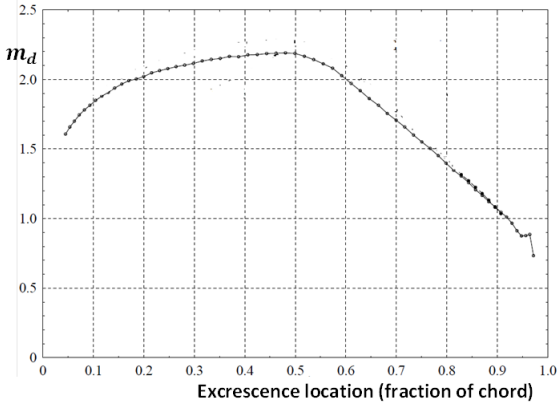

Fig. 8 Magnification factor, m_d, calculated using VGK (RAE 2822 aerofoil, upper surface, $M_\infty = 0.75, C_L = 0.5$). Reference [9]

Fig. 8 shows the magnification factor calculated using VGK for various excrescence locations on the upper surface of a RAE 2822 aerofoil running at supercritical conditions. For

a considerable extent the basic drag is more than doubled. This is of particular significance in the high-velocity region on the forward part of the wing where the basic excrescence drag is high because of high local kinetic pressure.

5 Wind-tunnel testing

The high standard of aerodynamic prediction required for transonic transport aircraft led to the introduction of large high-Reynolds-number transonic facilities, such as the ETW [10]. Such facilities are capable of full-scale Reynolds number testing but costs are very high and therefore they are only used when the aerodynamic design has reached a mature stage.

Cheaper tests in lower Reynolds number facilities are useful at an intermediate design stage but, as maximum test Reynolds numbers may be an order of magnitude lower than full scale, careful extrapolation is needed.

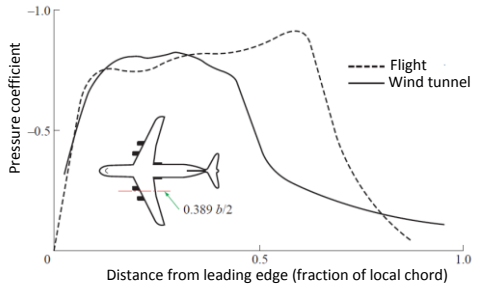

Fig. 9 Wind tunnel prediction of shock location [11]

Fig. 9 shows the difference in shock-wave location on a transonic wing measured both in flight and in a wind-tunnel test at low Reynolds number. Gross errors, due to the influence of Reynolds number on the shock/boundary-layer interaction, are apparent in the wind-tunnel prediction. Fig. 10 illustrates schematically a typical variation of lift coefficient with Reynolds number. Between A and C there is a rapid change corresponding to a large movement in the shock location. From C to D the shock position is stable and there is a much smaller variation in lift coefficient. A to B represents the available wind-tunnel test range.

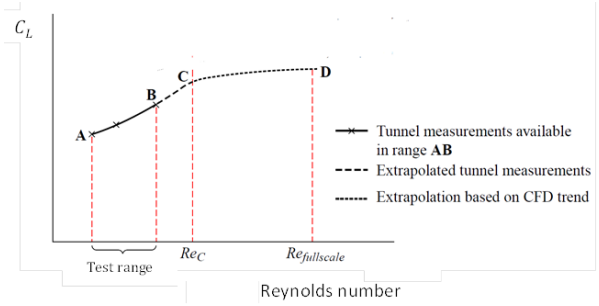

Fig. 10 Variation of lift coefficient, C_L, with effective Reynolds number

In order to avoid the unrepresentative laminar boundary-layer regions that occur in a low-Reynolds-number test on a swept-wing configuration, it is common to induce transition by using roughness (transition) strips near the wing leading edge. However this leads to an unrepresentatively thick turbulent boundary layer and poor modelling of full-scale features such as the shock/boundary layer interaction.

References [12] and [13] describe how increased effective Reynolds numbers may be simulated by placing the transition strip at greater distances from the leading edge to reduce the thickness of the turbulent boundary layer in sensitive locations, such as the shock/boundary-layer interaction region, thus giving a better match to full-scale conditions*.

In order to use this technique to construct the curve in A to B (Fig. 10) it is necessary to map the transition strip location to an effective Reynolds number that reflects the reduced boundary-layer thickness at the selected location. VGK or VFP offer a convenient way to achieve this mapping because transition can be directly imposed at a specified location within the laminar flow region at low Reynolds numbers. Thus, at the test Reynolds number, changes in the boundary-layer properties at a selected point on the wing caused by movement of the transition strip are easily modelled. Transition location is then mapped to the Reynolds number at which VGK/VFP gives similar boundary-layer properties with transition imposed near the leading edge.

* This reintroduces a laminar flow region that leads to the need for suitable correction to wind-tunnel drag measurements,

VGK or VFP can also be used to establish point C (Fig. 10) to which the wind-tunnel results are extrapolated [13]. VGK/VFP is then be used to extrapolate from C to full-scale Reynolds number (point D in Fig. 10).

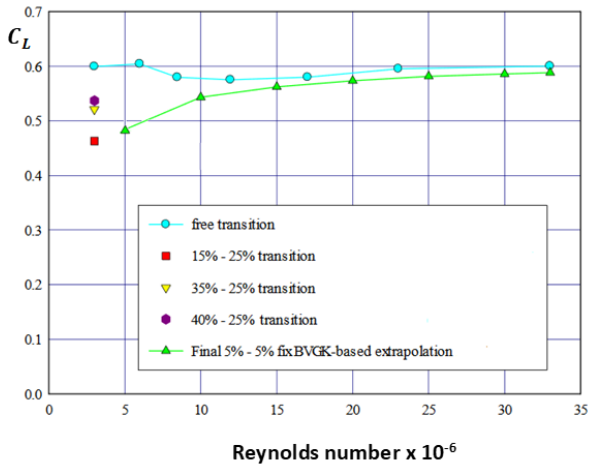

Fig. 11 Extrapolation of low-Reynolds number wind-tunnel test data using aft-fixing (adapted from [13])

Fig. 11 shows an example of low-Reynolds number test extrapolation using aft-fixing compared with a test on the same wing/body configuration tested with free transition over a large Reynolds number range in the ETW facility. The data for the low Reynolds-number tests, shown in Fig. 11, correspond to a Reynolds number of 3.0×10^6 with transition fixed at 25%, 35% and 40% of chord on the upper surface and fixed at 25% chord on the lower wing surface. Following the procedure outlined above, BVGK was used to match the experimental value at point C (Fig. 10) and then extrapolate further to the notional full-scale Reynolds number of 33.0×10^6. To allow for changes along the span, this process was done at three spanwise stations on the wing and the extrapolation shown in Fig. 11 is the result of combining these. The extrapolation agrees reasonably well with the full-Reynolds number test and the use of aft fixing gives a good idea of the flow characteristics at full-scale Reynolds number at reasonably low cost. A detailed account of this particular extrapolation is given in [14] and other scenarios and the choice of simulation criteria are described in [13] and its associated documents.

6 Conclusions

Viscous full-potential methods offer a number of advantages. Speed and automatic gridding make them particularly suitable for use in design optimisation procedures that demand a large number of repetitive calculations over a design space.

They are currently an integral tool in the assessment of excrescence drag because of the ease with which the local boundary-layer at an excrescence location can be modified to reflect the influence of the excrescence on the downstream flow on a lifting surface.

Integral boundary-layer modelling and its associated detailed output, together with the facility to fix transition location provides a useful tool with which to plan and extrapolate low-Reynolds-number wind-tunnel tests.

7 References

[1] ESDU, VGK method for two-dimensional aerofoil sections. Part 1: Principles and Results, *ESDU Transonic Data Memor. No. 96028 (with Amendment A and B)*, October 1996 ESDU, April 2004.

[2] Ashill P R, Wood R.F and Weeks D J. An improved, semi-inverse version of the viscous, Garabedian and Korn method (VGK). *RAE TR87002*, January 1987.

[3] ESDU, Viscous full-potential (VFP) method for three-dimensional wings and wing-body combinations. Part 1: Validation of VFP results with experiment and comparisons with other methods, *ESDU 13013*, ESDU, June 2014.

[4] ESDU, A method of determining the wave drag and its spanwise distribution on a finite wing in transonic flow. *ESDU Transonic Data Memor. 87003, (with Amendments A and B)*, February 1995.

[5] Green J E, Weeks D J and Brooman J W F, Prediction of turbulent boundary-layers and wakes in compressible flow by a lag-entrainment method. *ARC R & M 3791*, 1973.

[6] Doherty J J, Transonic airfoil study using sonic plateau, optimization and off-design performance Maps, *35th AIAA Applied Aerodynamics Conference*, Denver USA, 2017.

[7] Gaudet L and Winter K. Measurement of the drag of some characteristic aircraft excrescences immersed in turbulent boundary layers. *AGARD Conference Proceedings No. 124 on Aerodynamic Drag*, Izmir, Turkey, Paper 4-1, 1973.

[8] ESDU, An Introduction to aircraft excrescence drag, *ESDU 90024 (with amendments A to C)*, IHS Markit (ESDU), 2016.

[9] ESDU, VGK method for two-dimensional aerofoil sections, Part 4, estimation of excrescence drag at subsonic speeds, *ESDU 98031*, IHS (ESDU), 1998.
[10] Hefer G, ETW- A facility for high Reynolds number testing, *IUTAM Symposium Transsonicum IV*, Göttingen, Germany, 2002.
[11] Loving D L, Wind-tunnel-flight correlation of shock-induced separated flow, *NASA-TN-D-3580*, 1966.
[12] Laster, M.L. *et al*. Boundary layer simulation and control in wind tunnels, *AGARD advisory report 224 (AGARD-AR-224)*, 1988.
[13] ESDU, Extrapolating wind-tunnel data to full-scale Reynolds number, Part 1, procedures, *ESDU 07010*, IHS (ESDU), 1998.
[14] ESDU, Extrapolating wind-tunnel data to full-scale Reynolds number, Part 3: Example (ii) Comparison of extrapolated low-Reynolds-number lift measurements on the F4 wing/body with high-Reynolds-number measurements, *ESDU 11006*, IHS (ESDU), 2011.

8 Contact Author Email Address

mailto: david.philpott@ihsmarkit.com

Copyright Statement